

Article

Semi-Hydrogenation of Acetylene to Ethylene Catalyzed by Bimetallic CuNi/ZSM-12 Catalysts

Song Hu ^{1,*}, Chong Zhang ², Mingyu Wu ², Runping Ye ², Depan Shi ¹, Mujin Li ¹, Peng Zhao ¹, Rongbin Zhang ^{2,*} and Gang Feng ²

¹ State Key Laboratory of Green Chemical Engineering and Industrial Catalysis, Department of Process Development and Design, Shanghai Research Institute of Petrochemical Technology, Shanghai 201208, China

² Key Laboratory of Jiangxi Province for Environment and Energy Catalysis, Institute of Applied Chemistry, College of Chemistry and Chemical Engineering, Nanchang University, Nanchang 330031, China

* Correspondence: husong.sshy@sinopec.com (S.H.); rbzhang@ncu.edu.cn (R.Z.)

Abstract: The purpose of this work is to develop a low-cost and high-performance catalyst for the selective catalytic hydrogenation of acetylene to ethylene. Non-precious metals Cu and Ni were selected as active ingredients for this study. Using ZSM-12 as a carrier, Cu-Ni bimetallic catalysts of CuNi_x/ZSM-12 (x = 5, 7, 9, 11) with different Ni/Cu ratios were prepared by incipient wetness impregnation method. The total Cu and Ni loading were 2 wt%. Under the optimal reaction conditions, the acetylene conversion was 100%, and the ethylene selectivity was 82.48%. The CuNi₇/ZSM-12 prepared in this work exhibits good performance in the semi-hydrogenation of acetylene to ethylene with low cost and has potential for industrial application.

Keywords: acetylene; ethylene; selective hydrogenation; copper; nickel; bimetallic



Citation: Hu, S.; Zhang, C.; Wu, M.; Ye, R.; Shi, D.; Li, M.; Zhao, P.; Zhang, R.; Feng, G. Semi-Hydrogenation of Acetylene to Ethylene Catalyzed by Bimetallic CuNi/ZSM-12 Catalysts. *Catalysts* **2022**, *12*, 1072. <https://doi.org/10.3390/catal12091072>

Academic Editor: Leonarda Francesca Liotta

Received: 2 August 2022

Accepted: 15 September 2022

Published: 19 September 2022

Publisher's Note: MDPI stays neutral with regard to jurisdictional claims in published maps and institutional affiliations.



Copyright: © 2022 by the authors. Licensee MDPI, Basel, Switzerland. This article is an open access article distributed under the terms and conditions of the Creative Commons Attribution (CC BY) license (<https://creativecommons.org/licenses/by/4.0/>).

1. Introduction

Ethylene is a chemical in great demand for the preparation of downstream products [1,2]. Ethylene is usually obtained through the petrochemical route; that is, the catalytic cracking of petrochemical raw materials [3]. In recent years, with the continuous reduction of petroleum resources and the continuous increase of the demand for ethylene, people are exploring other methods to replace the petrochemical route to prepare ethylene. As we all know, China is a big country producing coal [4,5]. Thus, the synthesis of ethylene from the coal chemical route is a good alternative. The acetylene route based on calcium carbide is considered to be a very green and feasible production route [6].

At present, the most used active metal in hydrogenation reaction is Pd. Pd has extremely high activity for the conversion of acetylene, and 100% acetylene conversion can be achieved at relatively low temperatures [7]. “Recently, plenty of research focuses on the hydrogenation of acetylene to ethylene, such as the shale gas method [8], the electrochemical method [9], and Methanol to Olefins [10]. However, alloy catalysts are still the most widely used catalysts due to their excellent catalytic activity and selectivity [11].”

Besides active Pd being used in the selective hydrogenation of acetylene, it has been reported that other metals such as Pt [12,13], Ni [14–16], Au [17–19], Cu [20,21] can also be used as acetylene selection. The active metals of the hydrogenation catalysts and the order of their hydrogenation activity are: Pd > Pt > Ni > Au > Cu [22]. Pd and Pt are precious metals, and the resources are scarce, which is not conducive to extensive industrial application. Ni is a kind of non-precious metal discovered in recent years with good hydrogenation activity of acetylene, which has been widely studied by researchers [23]. Liu et al. [24] systematically studied the effect of different doping and different active metals on Ni-based catalysts, and adding IB (Group IB of the Periodic Table) metals to Ni-based catalysts can greatly improve the activity. The order of reactivity was: AuNi_{0.5}/SiO₂ > AgNi_{0.5}/SiO₂ > CuNi_{0.125}/SiO₂. Copper-based catalysts are less studied because of the

low activity of Cu for acetylene hydrogenation. However, copper-based catalysts exhibit excellent selectivity towards ethylene at high temperatures. Monometallic Cu catalysts are easy to cause the polymerization of acetylene, and the polymer of acetylene would block the catalyst pores [25]. Thus, copper catalysts generally need to be modified by adding doping metals.

There are also many studies on nickel-based catalysts for acetylene hydrogenation, especially for the bimetallic catalysts. Many metal promoters have been added to Ni-based catalysts toward regulating the performance of acetylene hydrogenation. Wang et al. [26] prepared Ni-based catalysts and doped Ga with different Ni/Ga ratios. The results show that the selectivity of ethylene was better when Ni/Ga was 5. The enhanced performance was attributed to the formed Ni-Ga alloy and Ni₃Ga intermetallic compound. Currently, there is charge transfer between Ni and Ga, which is beneficial to reduce the adsorption strength and adsorption capacity of ethylene on Ni atoms, then inhibit the peroxidation reaction and ethylene polymerization, and improve the selectivity of ethylene. However, the acidity and strength of the catalyst tended to increase with the increase of Ga content, which promotes polymerization and carbon deposition, which easily leads to catalyst deactivation. Chen et al. [27] prepared Ni/SiO₂, Ni-In/SiO₂ and Ni-In-K/SiO₂ catalysts by the impregnation method and found that the addition of tin can significantly improve the conversion rate of acetylene, the selectivity of ethylene and also the catalytic stability. The main reason was that the geometric effect of In causes continuous Ni atoms to be isolated, and the electronic effect of In and Ni produces electron transfer to put Ni in an electron-rich state, while adding K would improve the selectivity of ethylene. In fact, due to the isolation effect and the transfer of electrons, the hydrogenolysis of C=C and the polymerization of acetylene were inhibited, and the surface acid strength and acid content of the catalyst were weakened. Hu et al. [14] prepared a Ni-Cu/Al₂O₃ catalyst with a Ni/Cu ratio of 1:1 by co-precipitation for the selective hydrogenation of acetylene to ethylene, resulting in nearly 100% acetylene conversion and 71% ethylene selectivity.

Although the metal oxide supported bimetallic NiCu catalyst has been investigated, the zeolites supported NiCu catalysts have been less investigated [28]. Komatsu et al. used MCM-41 molecular sieve with a mesoporous diameter as the support to prepare a uniformly dispersed Ni₃Ge bimetallic catalyst. Compared with the traditional SiO₂ carrier, MCM-41-supported Ni₃Ge exhibited greater activity for the hydrogenation of cyclohexene. This is mainly due to the confinement effect between the Ni₃Ge particles and the pore wall. This constraint effect is more obvious for MCM-41 with a smaller pore diameter [29]. Huang et al. modified β-zeolite with K⁺, and the modified β-zeolite had higher ethylene selectivity compared with γ-Al₂O₃ and Na⁺-β-zeolite supports, mainly due to the preference for acetylene over ethylene. Adsorbed on the modified β-zeolite [30].

In this study, ZSM-12 was chosen as the support due to its good thermal stability, unique pore structure and regulated acidity. Besides, a single molecular sieve was not active for acetylene hydrogenation. We choose the non-precious metal Ni as the active component, but the noble metal Ni often leads to excessive hydrogenation of acetylene to ethane due to its high activity. Therefore, in this work, we use NiCu bimetallic as the active component of the catalyst, which is supported on ZSM-12 support, and compared with single Ni/ZSM-12, the effect of Cu composition on catalyst performance was studied.

2. Results and Discussions

2.1. Catalyst Characterizations

To understand the phase composition of the catalysts, XRD characterization of H-ZSM-12 support, CuNi_x/ZSM-12 and reduced catalyst is shown in Figure 1. The XRD pattern of H-ZSM-12 support shows that it presents typical diffraction peaks of H-ZSM-12, indicating that the support has been successfully synthesized. After loading different ratio CuNi_x/ZSM-12 catalysts, they also only presented the characteristic diffraction peaks of H-ZSM-12 support, without showing the diffraction peaks of NiO or CuO. It suggests that the metal with low loading was highly dispersed on the carrier and the impregnation

method would not destroy the support's structure. The reduction process at 500 °C did not affect the structure of the catalyst, only showing H-ZSM-12. The characteristic diffraction peak and the structure of the catalyst did not change after the stability test, indicating the excellent stability of the catalyst.

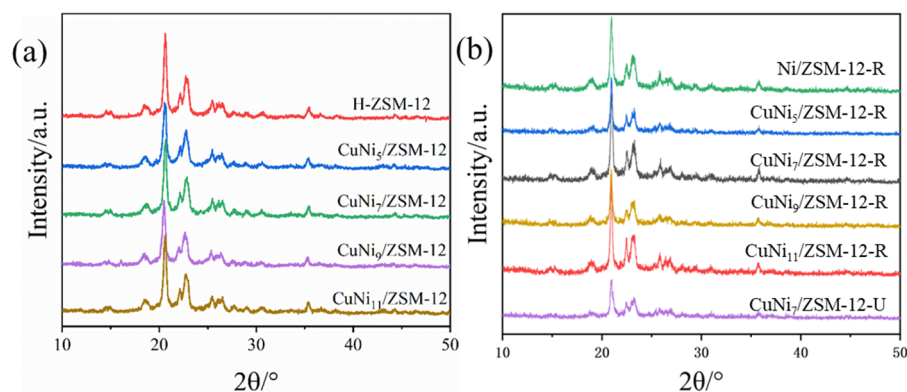


Figure 1. (a) XRD patterns of H-ZSM-12 and CuNi_x/ZSM-12 catalysts, (b) XRD patterns of the catalyst after reduction.

As shown in Figure 2, we carried out SEM and TEM analyses for the CuNi₇/ZSM-12 catalyst. According to the SEM images, the CuNi₇/ZSM-12 catalyst is a square nanoparticle with a rough surface. It can be seen from the TEM image that the metal compounds are uniformly distributed in the ZSM-12 on the surface of the carrier, which is consistent with the XRD and XPS results.

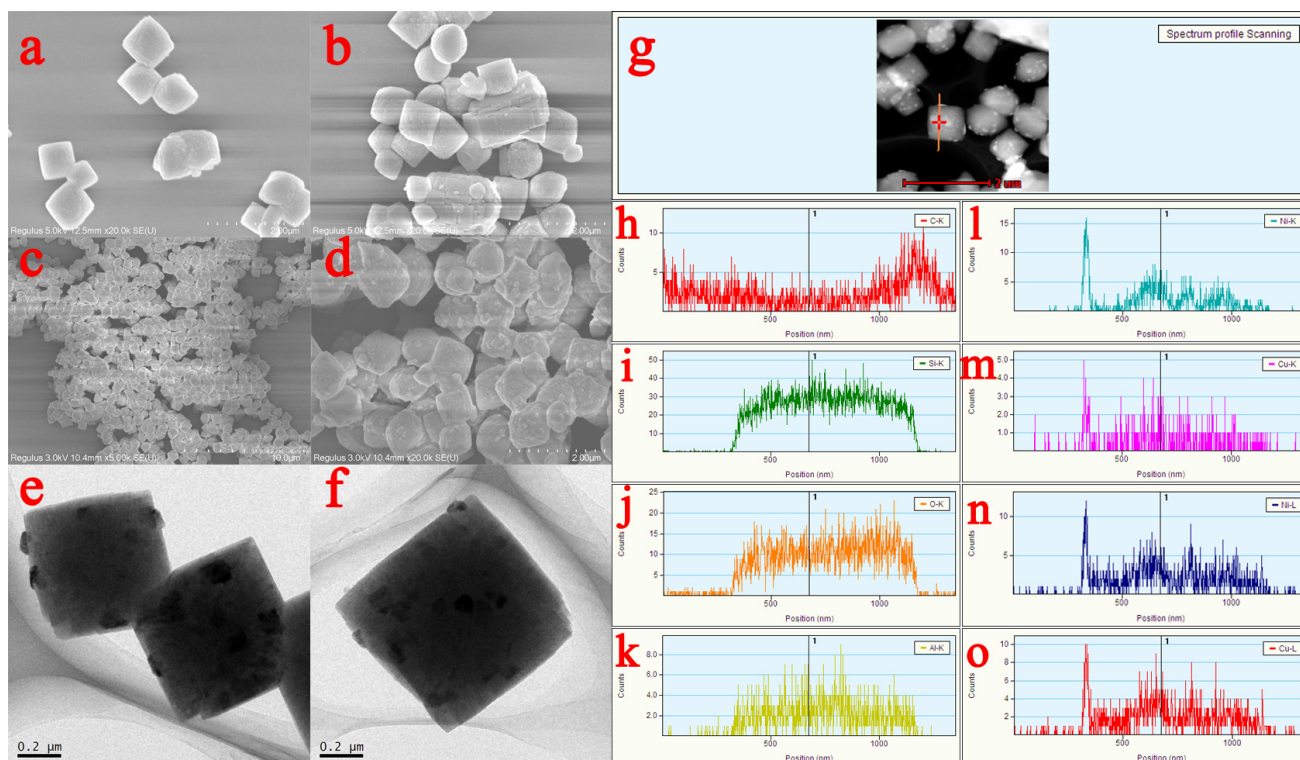


Figure 2. (a,b) The SEM results of Ni₇Cu/ZSM-12; (c,d) SEM results of Ni₇Cu/ZSM-12 after stability test; (e,f) the TEM results of Ni₇Cu/ZSM-12; (g–o) EDS line profile results of Ni₇Cu/ZSM-12.

Furthermore, N₂-adsorption and desorption experiments were carried out to characterize their specific surface area, pore structure and pore volume. As can be seen from Figure 3,

N_2 -adsorption and desorption curves of both the H-ZSM-12 support and $CuNi_x/ZSM-12$ ($x = 5, 7, 9, 11$) catalysts are IV isotherms with H4-type hysteresis loops, indicating that they have both microporous and mesoporous structures. According to the pore size distribution curves of the samples (Figure 3b), their pores are in the range of 3–4.5 nm, 4.5–15 nm, and below 2 nm. The pore size distribution is consistent with the N_2 -adsorption and desorption curve and indicates that the support and catalysts exhibit both microporous and mesoporous. The specific surface area (S_{BET}), pore volume (V_P) and average pore size (D_P) are listed in Table 1. It can be seen that the S_{BET} , V_P , and D_P values of the $CuNi_x/ZSM-12$ catalysts are slightly lower than those of the H-ZSM-12 support. Therefore, the Cu and Ni metals have been successfully loaded into the zeolite support. The inductively coupled plasma emission spectroscopy (ICP-AES) was further tested as the actual metal loading, as shown in Table 1. The actual atomic ratio of each catalyst is close to the theoretical metal loading and atomic ratio.

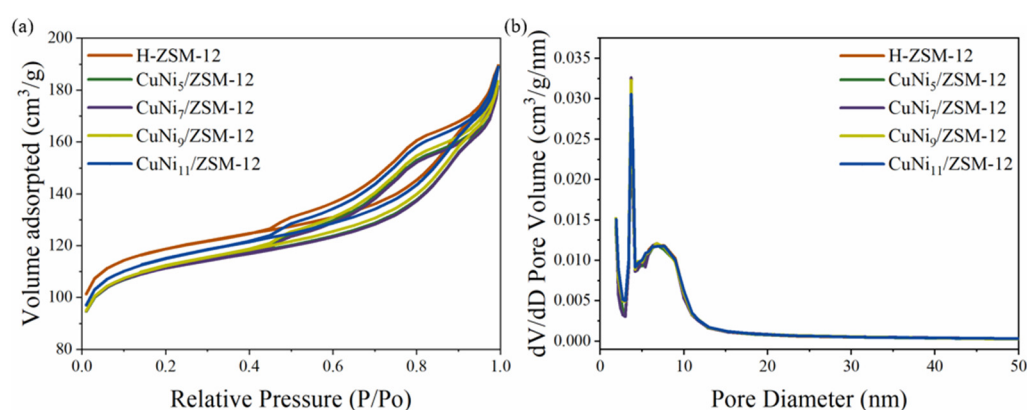


Figure 3. N_2 -adsorption/desorption curves (a) and pore size distributions (b) of H-ZSM-12 and $CuNi_x/ZSM-12$ catalysts.

Table 1. Structural information and metal loadings of prepared samples.

Samples	S_{BET} m ² /g	V_P cm ³ /g	D_P nm	Ni (wt%)	Cu (wt%)	Cu/Ni
$CuNi_5/ZSM-12$	361.7	0.142	6.987	1.56	0.34	5.04
$CuNi_7/ZSM-12$	361.9	0.139	7.236	1.73	0.27	6.91
$CuNi_9/ZSM-12$	365.0	0.140	6.858	1.80	0.21	9.46
$CuNi_{11}/ZSM-12$	374.2	0.144	6.952	1.82	0.17	11.65
H-ZSM-12	385.8	0.149	7.093	-	-	-

The H_2 -TPR curves of Ni/ZSM-12, Cu/ZSM-12 and $CuNi_x/ZSM-12$ catalysts were studied, as shown in the Figure 4, and Ni/ZSM-12 showed a broad peak at 250.69 °C to 530.19 °C that attributed to the reduction of NiO species [3,31]. Cu/ZSM-12 appeared at two peaks at 198.42 °C and 246.96 °C, which were assigned to the reduction of Cu^{2+} and Cu^+ species, respectively [21]. The $CuNi_x/ZSM-12$ series catalysts exhibited a large broad peak. The peak at low temperature belongs to the reduction of Cu species, and the peak at higher temperature is owing to the reduction of Ni species. Moreover, all the peaks shifted toward lower temperatures with the increase in Cu loading. It is shown that there is a strong interaction between Ni and Cu species, forming intermetallic compounds [15].

Furthermore, we used XPS to analyze the chemical states and surface properties of Ni/ZSM-12, Cu/ZSM-12, and $CuNi_7/ZSM-12$ catalysts. As illustrated in Figure 5a, the Ni2p peaks of Ni/ZSM-12 and $CuNi_7/ZSM-12$ catalysts can be deconvoluted into three components consisting of Ni satellite, Ni^{2+} , and Ni^0 [32]. The Ni/ZSM-12 exhibits a higher intensity than $CuNi_7/ZSM-12$ and the three peaks have a slight red shift after $CuNi_7$ formation, which means that the Cu doping has a strong interaction with Ni and produces an apparent electronic transfer. The Cu 2p peaks of Cu/ZSM-12 and $CuNi_7/ZSM-12$ catalysts are presented in Figure 5b, the binding energy peaks around 935 and 955 eV

belong to the Cu 2p_{3/2} and Cu 2p_{1/2} states, respectively [33]. The CuNi₇/ZSM-12 contains fewer Cu species, and the ratio of Cu²⁺, Cu⁰/Cu⁺ is different from Cu/ZSM-12, which suggests the chemical states of Cu are different.

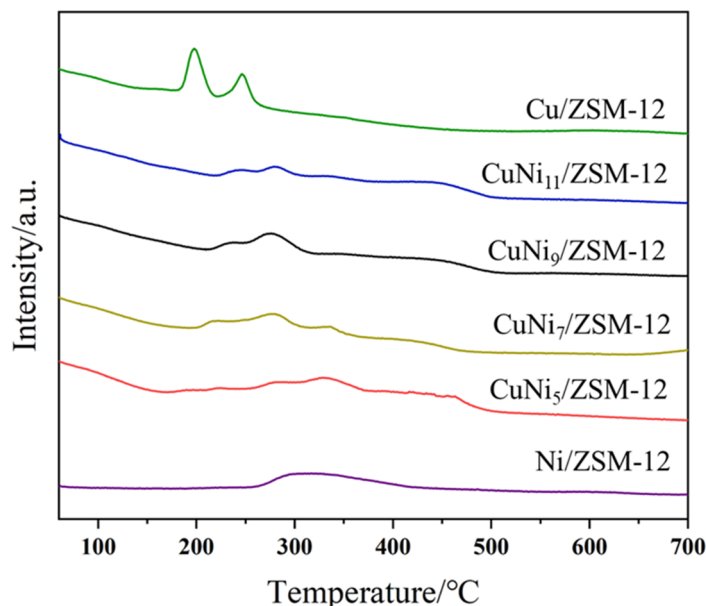


Figure 4. H₂-TPR results of CuNi_x/ZSM-12, Cu/ZSM-12 and Ni/ZSM-12 catalysts.

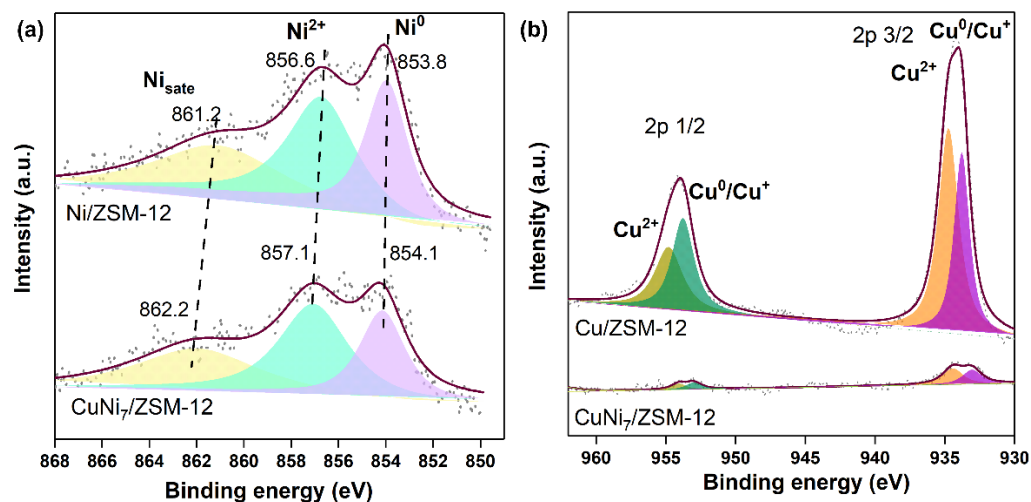


Figure 5. XPS spectra of Ni2p (a) of Ni/ZSM-12 and CuNi₇/ZSM-12 catalysts; Cu2p (b) of Cu/ZSM-12 and Ni/ZSM-12, Cu/ZSM-12 and CuNi₇/ZSM-12 catalysts.

To investigate the acidity of these catalysts, the catalysts were characterized by NH₃-TPD. As can be seen from the Figure 6 and Table 2, all the catalysts perform two similar peaks. The low-temperature peak is around 110 °C, while the high-temperature peak appears at 356 °C, which corresponds to weak and moderately strong acids, respectively [26]. Compared with Ni/ZSM-12, the medium and strong acid sites of Cu/ZSM-12 prefer lower temperatures. It indicates that the Ni-based catalyst contains less acidic sites and adding Cu component on Ni-based catalyst would reduce the total acid amount and catalyst acid strength.

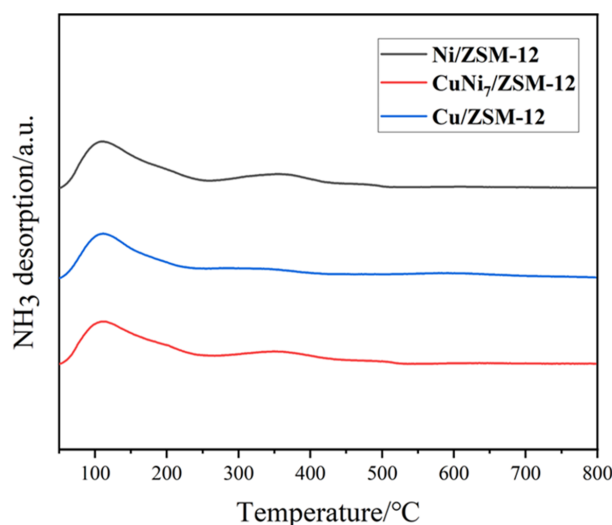


Figure 6. NH_3 -TPD results of Ni/ZSM-12, $\text{CuNi}_7/\text{ZSM-12}$ and Cu/ZSM-12.

Table 2. Relative acid amounts of different catalysts.

Samples	Relative Acidity Amount		
	I (a)	II (a)	Total Acid
Ni/ZSM-12	1	0.41	1.41
$\text{CuNi}_7/\text{ZSM-12}$	0.94	0.38	1.32
Cu/ZSM-12	0.91	0.27	1.18

(a): I stands for weak acid in the first peak while II stands for medium strong acid in the second peak.

2.2. Catalytic Performance of 2 wt% Cu/ZSM-12 and 2 wt% Ni/ZSM-12

The catalytic performance of Ni and Cu supported by ZSM-12 is shown in Figure 7. The activity of pure 2 wt% Cu/ZSM-12 catalyst for acetylene hydrogenation was very low, and there was almost no activity before 150 °C. Then it increased with the increase of temperature above 150 °C, but the acetylene conversion was still only 59.59% at 250 °C over 2 wt% Cu/ZSM-12. The selectivity toward ethylene was also increased with increasing the reaction temperature, but it could reach up to 78.54% at 250 °C over 2 wt% Cu/ZSM-12. For the 2.0 wt% Ni/ZSM-12 catalyst, the acetylene conversion was 100% at above 90 °C. However, the selectivity of ethylene was not high, and it increased with the increase in temperature, which was only 70.53% at 250 °C. Thus, it was necessary to combine 2.0 wt% Cu/ZSM-12 and 2.0 wt% Ni/ZSM-12 catalysts.

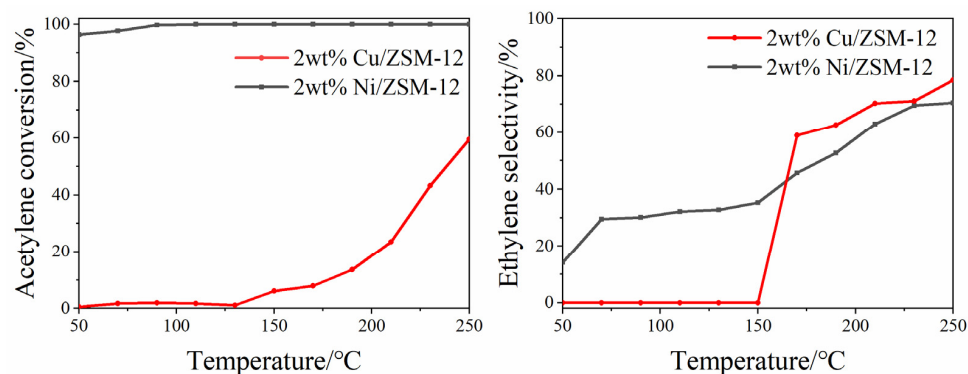


Figure 7. Catalytic performance of 2 wt% Cu/ZSM-12 and 2 wt% Ni/ZSM-12.

2.3. Catalytic Performance of $\text{CuNi}_x/\text{ZSM-12}$ Catalysts

Figure 8 shows the catalytic performance of ZSM-12 with different CuNi ratios, $\text{CuNi}_x/\text{ZSM-12}$ ($x = 5, 7, 9, 11$) catalysts have high catalytic activity for acetylene hy-

drogenation, with the acetylene conversion reaching more than 95% at 90 °C and 100% after 110 °C. For ethylene selectivity, the CuNi₅/ZSM-12 and CuNi₇/ZSM-12 catalysts presented higher selectivity to ethylene than the other samples. At 250 °C, CuNi₇/ZSM-12 catalyst exhibited the highest selectivity to ethylene (82.48%) and acetylene conversion reached up to 100%. Compared with pure 2.0 wt% Cu/ZSM-12 and 2.0 wt% Ni/ZSM-12, the catalytic performance—especially the ethylene yield of CuNi₇/ZSM-12 for acetylene hydrogenation—was much better. Thus, the Cu promoter could increase the ethylene yield. At the same time, we also compared with the catalysts reported in other literatures (see Table S1), the CuNi bimetallic catalysts studied in this paper show better catalytic performance than other Ni-based catalysts, which are close to the catalytic performance of noble metal catalysts performance, providing an interesting proposal for the study of non-precious metal catalysts.

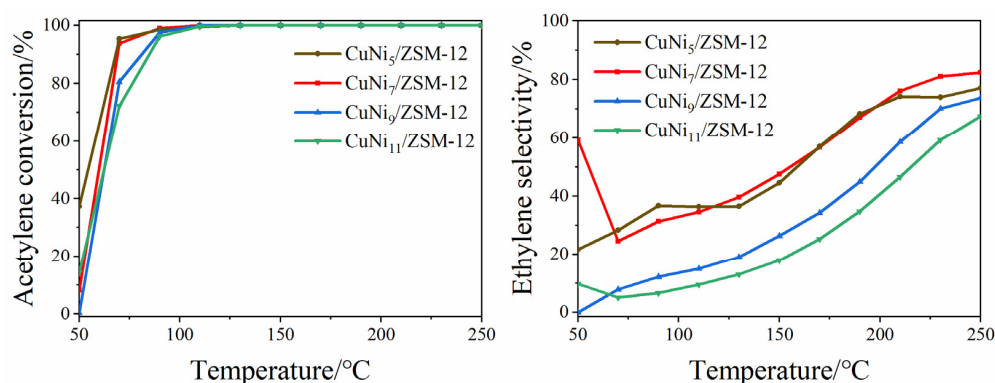


Figure 8. Activity test results of catalyst CuNi_x/ZSM-12 (x = 5, 7, 9, 11).

In addition, the influence of the ratio of hydrogen to alkyne on catalytic performance of CuNi₇/ZSM-12 catalyst was investigated to find the optimal reaction conditions. Figure 9 shows that CuNi₇/ZSM-12 catalyzes the semi-hydrogenation of acetylene under a different ratio of hydrogen and alkyne. When the ratio of hydrogen to alkyne was one, acetylene conversion rate was lower than 20% and the selectivity of ethylene was also lower than 10%. This may be caused by a lack of hydrogen, and a large amount of acetylene was unable to be hydrogenated. Instead, some polymer would be generated and blocked catalysts. After 170 °C, the catalytic performance became deactivated. When the ratio of H₂/C₂H₂ increased to greater than or equal to two, the acetylene conversion could be largely increased to 100%. However, the selectivity of ethylene decreased with the increase of H₂/C₂H₂ ratio, which may be caused by the increase of hydrogen concentration and the excessive hydrogenation of acetylene to ethane. In general, the CuNi₇/ZSM-12 catalyst could selectively hydrogenate acetylene to ethylene with the ratio of H₂/C₂H₂ at two.

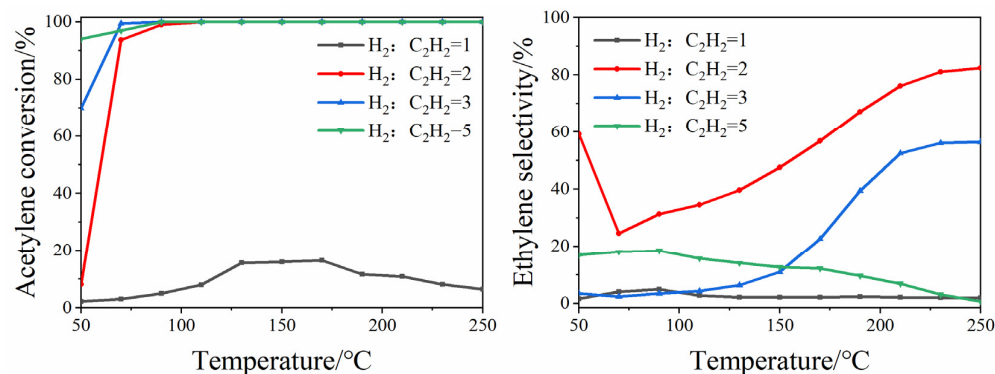


Figure 9. Influence of the hydrogen alkyne ratio on catalytic performance of CuNi₇/ZSM-12.

2.4. Catalytic Stability Test of CuNi₇/ZSM-12 Catalysts

The CuNi₇/ZSM-12 catalyst was tested at the highest yield the stability test, as shown in the Figure 10a, shows that the conversion of CuNi₇/ZSM-12 to acetylene has been maintained at 100%, and the selectivity of ethylene has been maintained at more than 80% before three hours, and after seven hours, the ethylene Selectivity was kept at 55%. TG analysis was performed on the catalysts before and after the reaction, as shown in the Figure 10b; for the fresh catalyst, the weight loss before 100 °C was attributed to the evaporation of water and remained constant thereafter, indicating the stability of the catalyst structure. For the reacted catalyst, the weight loss at 300–600 °C was attributed to the combustion of carbon deposits, which was the main reason for catalyst deactivation. The samples after stability test were analyzed by XRD and SEM. As shown in Figures 1 and 2, it can be seen that the crystal structure of the catalyst has not changed, but the catalyst agglomerates together, which is the main factor for the decrease of catalyst selectivity.

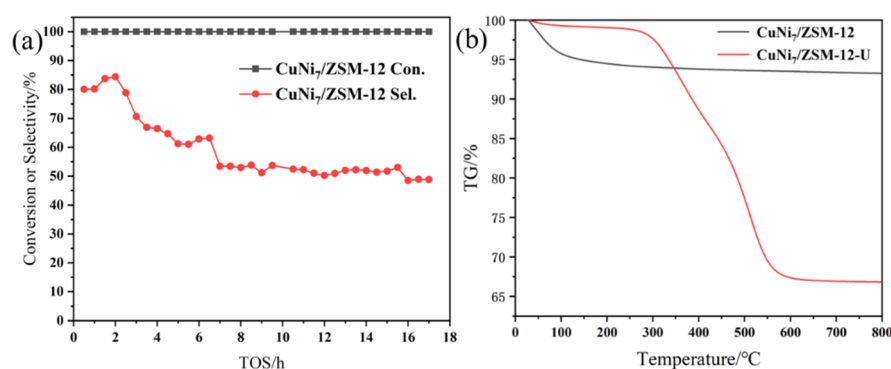


Figure 10. The stability test of CuNi₇/ZSM-12 catalyst for acetylene semi-hydrogenation to ethylene (a). Test conditions: P = 0.1 MPa, T = 250 °C, GHSV = 9000 mL·g⁻¹·h⁻¹, and TG results of CuNi₇/ZSM-12 before and after reaction (b).

3. Materials and Methods

3.1. Materials

CH₃CH₂OH (AR, China Sinopharm Group Chemical Reagent Co., Ltd., Ningbo, China), silica sol (40% SiO₂, China Shandong Haoyao New Material Co., Ltd., Shandong, China), tetraethylammonium hydroxide aqueous solution (25%, China Yancheng Fanan Chemical Co., Ltd., Yancheng, China), NaAlO₂ (AR, China Sinopharm Group Chemical Reagent Co., Ltd.), Ni(NO₃)₂·6H₂O (AR, China Tianjin Damao Chemical Reagent Factory, Tianjin, China), NH₄NO₃ (AR, China Taishan Yueqiao Reagent Plastic Co., Ltd., Taishan, China), Cu(NO₃)₂·3H₂O (AR, China Tianjin Damao Chemical Reagent Factory).

3.2. Carrier Preparation

ZSM-12 was prepared by hydrothermal synthesis. TEAOH, H₂O, NaAlO₂ and silica sol were added to the Teflon hydrothermal reaction kettle in turn and stirred for 0.5 h, then crystallized in an oven at 160 °C for six days. After crystallization, the products were washed and filtered with deionized water. The obtained solid products were dried at 60 °C overnight. The dried samples were roasted in a muffle furnace at 550 °C for 2 h and ground to obtain Na/ZSM-12, which was recorded as Na/ZSM-12. Finally, H-ZSM-12 was obtained by an ammonium ion exchange reaction of Na/ZSM-12.

3.3. Catalyst Preparation

The catalysts in this paper were prepared by the incipient wetness impregnation method. Preparation of single metal Cu or Ni/ZSM-12 catalysts with 2 wt% metal loading was as follows: 0.5 g of above ZSM-12 support was put in a crucible, then 0.5 mL solution of copper nitrate or nickel nitrate were slowly added to the carrier and dried naturally. The dried samples were calcined in a muffle furnace at 500 °C for 2 h. Finally, the samples

were named 2 wt% Cu/ZSM-12 and 2 wt% Ni/ZSM-12, respectively. For preparation of the bimetallic catalyst, take 0.5 g carrier in the crucible, mix the required volume of copper nitrate solution and nickel nitrate solution and take 0.5 mL of the mixed solution slowly added to the carrier; the solution should be a completely soaked carrier. Then, the samples are placed in a cool place for natural drying. After natural drying, the samples are roasted in a muffle furnace at 500 °C for 2 h. After roasting, the samples are ground to obtain a fresh catalyst. The CuNi_x/ZSM-12 catalysts (x is atomic ratio of Ni/Cu, x = 5, 7, 9, 11) were also prepared by the above method. The difference was that the single metal nitrate was changed to the corresponding copper nitrate and nickel nitrate. The total loading of Cu and Ni in the bimetallic catalysts were 2 wt%.

3.4. Catalyst Evaluation

The catalyst activity evaluation device used in this paper is a model 6010 small fixed-bed reactor. The flow speed of the reaction gas is controlled by the mass flowmeter developed by Beijing Seven-star Hua Chuang Electronics (Beijing, China). After the reaction of the gas raw material, the tail gas is separated and analyzed online by FULI 9790 gas chromatograph with packed column of the Hao han 790 GC System (Tengzhou, China). For evaluation, a 0.1 g fresh catalyst was installed in a straight reaction quartz tube, and both ends were fixed with an appropriate amount of quartz cotton. The reactor temperature was raised to 500 °C at a rate of 5 °/min under hydrogen flow of 20 mL/min, and the catalyst was reduced at 500 °C for 2 h. After the reduction treatment, the reaction gas acetylene and hydrogen (H₂: 10 mL/min, C₂H₂: 5 mL/min) were introduced after the temperature was cooled to 30 °C, and the space speed was 9000 mL·g_{cat}⁻¹·h⁻¹. For the detection of outlet steam composition at different reaction temperatures, acetylene conversion ($X_{C_2H_2}$) was calculated as follows:

$$X_{C_2H_2} = \frac{n_{C_2H_2(IN)} - n_{C_2H_2(OUT)}}{n_{C_2H_2(IN)}} \times 100\% \quad (1)$$

In the above formula, $X_{C_2H_2}$ is the acetylene conversion rate, $n_{C_2H_2(IN)}$ represents the acetylene injection amount, and $n_{C_2H_2(OUT)}$ represents the acetylene outflow amount detected by gas chromatography.

Ethylene selectivity ($S_{C_2H_4}$) was calculated as follows:

$$S_{C_2H_4} = \frac{n_{C_2H_4(OUT)}}{n_{C_2H_2(IN)} - n_{C_2H_2(OUT)}} \times 100\% \quad (2)$$

In the above formula, $S_{C_2H_4}$ is ethylene selectivity, $n_{C_2H_4(OUT)}$ is ethylene outflow detected by gas chromatography, $n_{C_2H_2(IN)}$ is acetylene injection volume, $n_{C_2H_2(OUT)}$ is acetylene outflow detected by gas chromatography.

Ethylene yield is calculated as follows:

$$Y_{C_2H_4} = X_{C_2H_2} \times S_{C_2H_4} \times 100\% \quad (3)$$

In the above formula, $Y_{C_2H_4}$ is the yield of ethylene, $X_{C_2H_2}$ is the conversion rate of acetylene and $S_{C_2H_4}$ is the selectivity of ethylene.

3.5. Catalyst Characterization

The X-ray diffractometer (XRD) (Beijing, China) was tested on an XD-3 X-ray diffractometer produced by Beijing General Analysis Instrument. The test conditions were as follows: the radiation source was Cu K α ($\lambda = 0.154$ nm) with the tube current of 30 mA and the radiation tube voltage of 40 kV. The data were collected in the 2 θ range of 10–50° at a scan speed of 4°/min. Determination of Ni and Cu content of samples was tested by the inductively coupled plasma emission spectroscopy (ICP-AES). The ICP instrument used in this paper is an Agilent 5100 ICP OES type inductively coupled plasma atomic emission

spectrometer produced by Agilent Technologies (Santa Clara, CA, USA). The physical adsorption tester used in this paper was done on an Micromeritics ASAP2020 physical adsorption tester. The physical adsorption tester used for the BET test was the Micromeritics ASAP2020 physical adsorption tester (Norcross, GA, USA). Hydrogen temperature-programmed reduction (H₂-TPR) was performed on a Chemisorb 2750 chemisorption instrument (Micromeritics Instrument Company, Norcross, GA, USA) equipped with a thermal conductivity detector (TCD). For the measurement of H₂-TPR, 50 mg of catalyst was charged in a U-shaped quartz tube reactor and reduced from 45 °C to 800 °C at a heating rate of 10 °C/min under 10 V% H₂-Ar. The SEM electron microscope tested in this paper is a JSM-6701F Field Emission Scanning Electron Microscope (FE-SEM) instrument produced by Hitachi, Tokyo, Japan. The secondary electron image resolution of the electron microscope is as follows: 1 nm (15 kV) and 2.2 nm (1 kV), magnifications are × 25–100,000, acceleration voltages are 0.5–30 kV. In this paper, the samples were characterized using Talos F200X field emission transmission electron microscope (TEM), the point resolution was less than 0.24 nm, the line resolution was less than 0.14 nm, and the voltage was 200 kV. Thermogravimetric (TG) analysis was performed on a TGA 550 instrument (TA Instruments, New Castle, DE, USA) under an air flow with a heating rate of 10 °C/min. NH₃ temperature programmed desorption (NH₃-TPD) was tested by Micromeritics AutoChem II 2920, the reduction temperature was 500 °C, and the heating rate was 10 °C/min. The measurement of the degree of dispersion was carried out using Micromeritics AutoChem II 2920 in the United States, and it was determined by hydrogen-oxygen titration. X-ray photoelectron spectroscopy (XPS) was performed on an Thermo Scientific K-Alpha instrument (Waltham, MA, USA) using Al K α radiation (1486.6 eV).

4. Conclusions

The pure Cu/ZSM-12 and Ni/ZSM-12 catalysts, as well as bimetallic CuNi_x/ZSM-12 catalysts, were prepared by impregnation method. The different nickel-copper ratio and hydrogen-acetylene ratio on the hydrogenation of acetylene to ethylene were investigated in detail. For the CuNi_x/ZSM-12 (x = 5, 7, 9, 11) catalysts, the CuNi₇/ZSM-12 catalyst with nickel-copper ratio of 7 displayed the best performance at 250 °C, with acetylene conversion reaching up to 100% and ethylene selectivity reaching up to 82.48%, which is much better than the performance of single-metal nickel and single-metal copper catalysts. In addition, it was found that the optimal ratio of H₂/C₂H₂ was two. The higher ratio of H₂/C₂H₂ would decrease the selectivity of ethylene, while the lower ratio of H₂/C₂H₂ would decrease the acetylene conversion. In summary, the copper promoter and the ratio of reactants would significantly affect the semi-hydrogenation of acetylene.

Supplementary Materials: The following supporting information can be downloaded at: <https://www.mdpi.com/article/10.3390/catal12091072/s1>, Table S1: Comparison of the activity and TOF of different catalysts that previous reports. References [34–43] are cited in Supplementary Materials.

Author Contributions: Writing—original draft preparation, S.H. and C.Z.; writing—review and editing, M.W., R.Y., D.S., M.L., P.Z., G.F. and R.Z.; project administration, S.H. and R.Z. All authors have read and agreed to the published version of the manuscript.

Funding: This work is grateful for the support of the National Natural Science Foundation of China (Grants No. 21875096 and U19B60021005505), the Foundation of State Key Laboratory of Coal Conversion (Grant No. J22-23-903) and the Natural Science Foundation of Jiangxi Province, China (Grants No. 20181BCD40004).

Data Availability Statement: The data presented in this study are available on request from corresponding authors.

Acknowledgments: The authors are also thankful for Shiyanjia Lab (www.shiyanjia.com) on the TEM, XPS, and TG analysis.

Conflicts of Interest: The authors declare no conflict of interest.

References

1. Hu, T.-L.; Wang, H.; Li, B.; Krishna, R.; Wu, H.; Zhou, W.; Zhao, Y.; Han, Y.; Wang, X.; Zhu, W. Microporous metal–organic framework with dual functionalities for highly efficient removal of acetylene from ethylene/acetylene mixtures. *Nat. Commun.* **2015**, *6*, 1–9. [[CrossRef](#)] [[PubMed](#)]
2. Gao, Y.; Neal, L.; Ding, D.; Wu, W.; Baroi, C.; Gaffney, A.M.; Li, F. Recent advances in intensified ethylene production—a review. *ACS Catal.* **2019**, *9*, 8592–8621. [[CrossRef](#)]
3. Li, Q.; Wang, Y.; Skoptsov, G.; Hu, J. Selective hydrogenation of acetylene to ethylene over bimetallic catalysts. *Ind. Eng. Chem. Res.* **2019**, *58*, 20620–20629. [[CrossRef](#)]
4. Gui, X.; Liu, J.; Cao, Y.; Miao, Z.; Li, S.; Xing, Y.; Wang, D. Coal preparation technology: Status and development in China. *Energy Environ.* **2015**, *26*, 997–1013. [[CrossRef](#)]
5. Zhang, X.; Song, X.; Wang, J.; Su, W.; Zhou, B.; Bai, Y.; Yu, G. Physico-chemical structure evolution characteristics of coal char during gasification in the presence of iron-based waste catalyst. *Int. J. Coal Geol.* **2020**, *7*, 456–463. [[CrossRef](#)]
6. Schobert, H. Production of acetylene and acetylene-based chemicals from coal. *Chem. Rev.* **2014**, *114*, 1743–1760. [[CrossRef](#)]
7. Ball, M.R.; Rivera-Dones, K.R.; Gilcher, E.B.; Ausman, S.F.; Hullfish, C.W.; Lebrón, E.A.; Dumesic, J.A. AgPd and CuPd catalysts for selective hydrogenation of acetylene. *ACS Catal.* **2020**, *10*, 8567–8581. [[CrossRef](#)]
8. Thiruvenkataswamy, P.; Eljack, F.T.; Roy, N.; Mannan, M.S.; El-Halwagi, M.M. Safety and techno-economic analysis of ethylene technologies. *J. Loss Prev. Process Ind.* **2016**, *39*, 74–84. [[CrossRef](#)]
9. Wang, S.; Uwakwe, K.; Yu, L.; Ye, J.; Zhu, Y.; Hu, J.; Chen, R.; Zhang, Z.; Zhou, Z.; Li, J. Highly efficient ethylene production via electrocatalytic hydrogenation of acetylene under mild conditions. *Nat. Commun.* **2021**, *12*, 1–9. [[CrossRef](#)]
10. Tian, P.; Wei, Y.; Ye, M.; Liu, Z. Methanol to olefins (MTO): From fundamentals to commercialization. *ACS Catal.* **2015**, *5*, 1922–1938. [[CrossRef](#)]
11. Pei, G.X.; Liu, X.Y.; Wang, A.; Lee, A.F.; Isaacs, M.A.; Li, L.; Pan, X.; Yang, X.; Wang, X.; Tai, Z. Ag alloyed Pd single-atom catalysts for efficient selective hydrogenation of acetylene to ethylene in excess ethylene. *ACS Catal.* **2015**, *5*, 3717–3725. [[CrossRef](#)]
12. Ma, H.-Y.; Wang, G.-C. Selective Hydrogenation of Acetylene on Pt n/TiO₂ (n = 1, 2, 4, 8) Surfaces: Structure Sensitivity Analysis. *ACS Catal.* **2020**, *10*, 4922–4928. [[CrossRef](#)]
13. Chesnokov, V.; Svintsitskii, D.; Chichkan, A.; Parmon, V. Effect of the structure of carbon support on the selectivity of Pt/C catalysts for the hydrogenation of acetylene to ethylene. *Nanotechnol. Russ.* **2018**, *13*, 246–255. [[CrossRef](#)]
14. Hu, N.; Yang, C.; He, L.; Guan, Q.; Miao, R. Ni–Cu/Al₂O₃ catalysts for the selective hydrogenation of acetylene: A study on catalytic performance and reaction mechanism. *New J. Chem.* **2019**, *43*, 18120–18125. [[CrossRef](#)]
15. Zhou, S.; Kang, L.; Zhou, X.; Xu, Z.; Zhu, M. Pure acetylene semihydrogenation over Ni–Cu bimetallic catalysts: Effect of the Cu/Ni ratio on catalytic performance. *Nanomaterials* **2020**, *10*, 509. [[CrossRef](#)] [[PubMed](#)]
16. Liu, Y.; Zhao, J.; Feng, J.; He, Y.; Du, Y.; Li, D. Layered double hydroxide-derived Ni–Cu nanoalloy catalysts for semi-hydrogenation of alkynes: Improvement of selectivity and anti-coking ability via alloying of Ni and Cu. *J. Catal.* **2018**, *359*, 251–260. [[CrossRef](#)]
17. Yang, B.; Burch, R.; Hardacre, C.; Headdock, G.; Hu, P. Origin of the Increase of Activity and Selectivity of Nickel Doped by Au, Ag, and Cu for Acetylene Hydrogenation. *ACS Catal.* **2012**, *2*, 1027–1032. [[CrossRef](#)]
18. Liu, X.; Li, Y.; Lee, J.W.; Hong, C.-Y.; Mou, C.-Y.; Jang, B.W. Selective hydrogenation of acetylene in excess ethylene over SiO₂ supported Au–Ag bimetallic catalyst. *Appl. Catal. A Gen.* **2012**, *439*, 8–14. [[CrossRef](#)]
19. Gluhoi, A.C.; Bakker, J.W.; Nieuwenhuys, B.E. Gold, still a surprising catalyst: Selective hydrogenation of acetylene to ethylene over Au nanoparticles. *Catal. Today* **2010**, *154*, 13–20. [[CrossRef](#)]
20. Chen, Y.; Liu, L.; Liu, B.-J. Selective hydrogenation of acetylene on CuNi/Al₂O₃ catalyst. *Chem. Eng. J.* **2012**, *32*, 50–52.
21. McCue, A.J.; McRitchie, C.J.; Shepherd, A.M.; Anderson, J.A. Cu/Al₂O₃ catalysts modified with Pd for selective acetylene hydrogenation. *J. Catal.* **2014**, *319*, 127–135. [[CrossRef](#)]
22. Ravanchi, M.T.; Sahebdehfar, S.; Komeili, S. Acetylene selective hydrogenation: A technical review on catalytic aspects. *Rev. Chem. Eng.* **2018**, *34*, 215–237. [[CrossRef](#)]
23. Ye, R.-P.; Liao, L.; Reina, T.R.; Liu, J.; Chevella, D.; Jin, Y.; Fan, M.; Liu, J. Engineering Ni/SiO₂ catalysts for enhanced CO₂ methanation. *Fuel* **2021**, *285*, 119151. [[CrossRef](#)]
24. Liu, H.; Chai, M.; Pei, G.; Liu, X.; Li, L.; Kang, L.; Wang, A.; Zhang, T. Effect of IB-metal on Ni/SiO₂ catalyst for selective hydrogenation of acetylene. *Chin. J. Catal.* **2020**, *41*, 1099–1108. [[CrossRef](#)]
25. Zhang, R.; Zhang, J.; Zhao, B.; He, L.; Wang, A.; Wang, B. Insight into the effects of Cu component and the promoter on the selectivity and activity for efficient removal of acetylene from ethylene on Cu-based catalyst. *J. Phys. Chem. C* **2017**, *121*, 27936–27949. [[CrossRef](#)]
26. Wang, L.; Li, F.; Chen, Y.; Chen, J. Selective hydrogenation of acetylene on SiO₂-supported Ni–Ga alloy and intermetallic compound. *J. Energy Chem.* **2019**, *29*, 40–49. [[CrossRef](#)]
27. Chen, Y.; Chen, J. Selective hydrogenation of acetylene on SiO₂ supported Ni–In bimetallic catalysts: Promotional effect of In. *Appl. Surf. Sci.* **2016**, *387*, 16–27. [[CrossRef](#)]
28. Zhao, J.; Hua, Z.; Liu, Z.; Li, Y.; Guo, L.; Bu, W.; Cui, X.; Ruan, M.; Chen, H.; Shi, J. Direct fabrication of mesoporous zeolite with a hollow capsular structure. *ChemComm* **2009**, *48*, 7578–7580. [[CrossRef](#)]
29. Komatsu, T.; Kishi, T.; Gorai, T. Preparation and catalytic properties of uniform particles of Ni₃Ge intermetallic compound formed inside the mesopores of MCM-41. *J. Catal.* **2008**, *259*, 174–182. [[CrossRef](#)]

30. Huang, W.; Pyrz, W.; Lobo, R.F.; Chen, J.G. Selective hydrogenation of acetylene in the presence of ethylene on K⁺-β-zeolite supported Pd and PdAg catalysts. *Appl. Catal. A Gen.* **2007**, *333*, 254–263. [[CrossRef](#)]
31. Zhou, S.; Kang, L.; Xu, Z.; Zhu, M. Catalytic performance and deactivation of Ni/MCM-41 catalyst in the hydrogenation of pure acetylene to ethylene. *RSC Adv.* **2020**, *10*, 1937–1945. [[CrossRef](#)] [[PubMed](#)]
32. Hu, F.; Chen, X.; Tu, Z.; Lu, Z.-H.; Feng, G.; Zhang, R. Graphene aerogel supported Ni for CO₂ hydrogenation to methane. *Ind. Eng. Chem. Res.* **2021**, *60*, 12235–12243. [[CrossRef](#)]
33. Li, A.; Yao, D.; Yang, Y.; Yang, W.; Li, Z.; Lv, J.; Huang, S.; Wang, Y.; Ma, X. Active Cu⁰-Cu^{σ+} Sites for the Hydrogenation of Carbon-Oxygen Bonds over Cu/CeO₂ Catalysts. *ACS Catal.* **2022**, *12*, 1315–1325. [[CrossRef](#)]
34. Zhou, H.; Yang, X.; Li, L.; Liu, X.; Huang, Y.; Pan, X.; Wang, A.; Li, J.; Zhang, T. PdZn intermetallic nanostructure with Pd-Zn-Pd ensembles for highly active and chemoselective semi-hydrogenation of acetylene. *ACS Catal.* **2016**, *6*, 1054–1061. [[CrossRef](#)]
35. Kang, J.H.; Shin, E.W.; Kim, W.J.; Park, J.D.; Moon, S.H. Selective Hydrogenation of Acetylene on TiO₂-Added Pd Catalysts. *J. Catal.* **2002**, *208*, 310–320. [[CrossRef](#)]
36. Kang, L.; Cheng, B.; Zhu, M. Pd/MCM-41 catalyst for acetylene hydrogenation to ethylene. *R. Soc. Open Sci.* **2019**, *6*, 191155. [[CrossRef](#)]
37. Zhou, S.; Shang, L.; Zhao, Y.; Shi, R.; Waterhouse, G.I.N.; Huang, Y.C.; Zheng, L.; Zhang, T. Pd Single-Atom Catalysts on Nitrogen-Doped Graphene for the Highly Selective Photothermal Hydrogenation of Acetylene to Ethylene. *Adv. Mater.* **2019**, *31*, e1900509. [[CrossRef](#)]
38. Jia, J.F.; Haraki, K.; Kondo, J.N.; Domen, K.; Tamaru, K. Selective hydrogenation of acetylene over Au/Al₂O₃ catalyst. *J. Phys. Chem. B* **2000**, *104*, 11153–11156. [[CrossRef](#)]
39. Sun, X.; Li, F.; Shi, J.; Zheng, Y.; Su, H.; Sun, L.; Peng, S.; Qi, C. Gold nanoparticles supported on MgO_x-Al₂O₃ composite oxide: An efficient catalyst for selective hydrogenation of acetylene. *Appl. Surf. Sci.* **2019**, *487*, 625–633. [[CrossRef](#)]
40. Pei, G.X.; Liu, X.Y.; Wang, A.; Su, Y.; Li, L.; Zhang, T. Selective hydrogenation of acetylene in an ethylene-rich stream over silica supported Ag-Ni bimetallic catalysts. *Appl. Catal. A-Gen.* **2017**, *545*, 90–96. [[CrossRef](#)]
41. Simanullang, W.F.; Ma, J.; Shimizu, K.-I.; Furukawa, S. Silica-decorated Ni-Zn alloy as a highly active and selective catalyst for acetylene semihydrogenation. *Catal. Sci. Technol.* **2021**, *11*, 4016–4020. [[CrossRef](#)]
42. Esmaili, E.; Mortazavi, Y.; Khodadadi, A.A.; Rashidi, A.M.; Rashidzadeh, M. The role of tin-promoted Pd/MWNTs via the management of carbonaceous species in selective hydrogenation of high concentration acetylene. *Appl. Surf. Sci.* **2012**, *263*, 513–522. [[CrossRef](#)]
43. Zhao, L.; Wei, Z.; Zhu, M.; Dai, B. Catalytic performance of a Ti added Pd/SiO₂ catalyst for acetylene hydrogenation. *J. Ind. Eng. Chem.* **2012**, *18*, 45–48. [[CrossRef](#)]